Coherent High-Speed Acoustic Communication Inside a Commercial Atlantic Salmon Pen

Email address: jacob.hiden.rudander@kongsberg.com (Jacob Rudander)

Coherent High-Speed Acoustic Communication Inside a Commercial Atlantic Salmon Pen

Jacob Rudander[a,c,*], Thor Husøy[a], Paul van Walree[b], Pål Orten[a,c]

[a] *Kongsberg Maritime, Horten Norway*
[b] *Norwegian Defence Research Establishment, Horten Norway*
[c] *University of Oslo, Oslo Norway*

Abstract

Fish telemetry is a potential method to monitor the well-being of farmed fish, where a reference group of fish are equipped with sensors tags that oversee their health and wirelessly transmit the data. Many fish must be tagged to get statistically reliable information. In this paper, very-high-frequency (250 kHz) acoustic channels are characterized using data recorded in an Atlantic salmon pen containing 180 000 fish. The results reveal vertical pen channels characterized by a direct path and a delayed tail of fluctuating multipath arrivals with an angular spread and a coherence time of order 14 ms. It is demonstrated that multichannel equalization applied to a 64-element hydrophone array enables high-speed (78 kbps) coherent communication in short bursts. We discuss the possibilities of using high-speed acoustic communication for fish telemetry and show that it has the potential of serving hundreds of distributed unsynchronized fish tags.

Keywords: Fish telemetry, aquaculture, high-speed communication, multichannel equalization, very-high-frequency, acoustic communication.

1. Introduction

Aquaculture is the fastest growing animal-based food producing sector in the world [1], and in 2016 46 % of the global fish (e.g. finfish, crustaceans, molluscs,

*Corresponding author
Email address: jacob.hiden.rudander@kongsberg.com (Jacob Rudander)

...) production came from aquaculture. This corresponds to 80 Mt, whereof the production of finfish alone stood for 54 Mt [1].

The most intensively farmed finfish in sea-based aquaculture is the Atlantic salmon, of which 2.2 Mt was produced in 2016 [1]. Smolt fish weighing 200 g are transferred from land-based facilities to sea-based net pens, where they stay and grow for another two years before they have reached their final weight of about 5 kg.

The most commonly used pens are of either rectangular or circular design with a circumference of up to 157 m and depth of 10–50 meters. There are typically several of such pens at each location, arranged in an array inside a fjord or calm bay, although an emerging approach is offshore pens [2], also known as open ocean aquaculture, using more robust or submerged pens. Stocking densities up to 25 kg/m^3 are common, which at the larger sites correspond to 200 000 Atlantic salmon per pen, or several millions of fish per site.

Keeping track of such a large number of animals is difficult, but necessary in order to respond to changes in the population or aquatic environment. Often such monitoring is required by legislation. Today most of the fish well-being [3] observations are done remotely by manual observations through cameras and echo sounders inside the pen or via on-site observation. The aquatic environment and the vast number of fish make this not only a difficult but also time-consuming task. The monitoring challenge will further increase with larger and less accessible, submerged, or open ocean pens. Another limitation with current observation methods is that they do not measure relevant quantities directly, but instead infer the conditions from behavioral and visible aspects.

With the ongoing work of precision fish farming [4], attempts are being made to apply control-engineering principles to fish farms. However, in order to control the biological processes with control engineering, access to relevant animal variables is required. This can be achieved by applying automated monitoring to fish farms, where fish telemetry is considered as an important enabling technology [4].

In fish telemetry [5, 6] individual fish are equipped with sensor tags, able

to measure and transmit properties of the environment near the fish, e.g. their position [e.g. 7, 8], depth [e.g. 9], swimming activity [e.g. 10, 9] or physiological factors as cardiac rhythm [e.g. 11]. Fish telemetry will, therefore, give valuable real-time information of the fishes' current status, compared with the indirect measurements based on behavioral observations provided by cameras and echo sounders. Provided that a sufficient number of representative fish are tagged, fish telemetry will be able to provide a statistically reliable assessment for the whole population.

Fish telemetry is not a new technology and is widely used in wild-fish research, for instance [11]. There have also been experiments with fish telemetry in fish farms [e.g. 7, 12, 9, 13, 14], where typically a standard off-the-shelf wild-fish system is used. However, the tag requirements for wild-fish research are very different from aquaculture monitoring. As pointed out by [4], the main limitations with available systems are 1) the complexity of tagging fish as this requires capturing the fish and surgery and 2) the poor communication performance. The present study focused on the second of these challenges.

Due to the strong attenuation of electromagnetic waves in seawater, acoustic communication is the preferred method for wireless underwater telemetry. The low sound speed of $\approx$ 1500 m/s can result in a large multipath delay spread and severe Doppler effects, [15]. In addition, there is strong attenuation at high frequencies [16] and high levels of ambient noise at low frequencies [17]. It is also interesting to note that even if the bandwidth in acoustic communication is limited to some tens of kilohertz, the acoustic channel is effectively an ultra-wideband channel since the carrier frequency is comparable to the bandwidth. In fish pens, there will be additional scattering effects due to the large moving biomass, and complete blocking of the acoustic signal may occur [9], in addition to platform movement induced by surface waves. Furthermore, the fish pen is a busy location with enhanced local ambient noise, at least in the low and mid-frequency range [18].

Available acoustic fish telemetry systems are typically based on single-input and multiple-output communication and exist with a variety of modulation

schemes and frequencies depending on the intended application. Fish tags can be pure ID tags or sensor tags that, in addition to ID transmit readings from attached sensors. An example of the use of pure ID tags is [7]. Here a fish localization system based on triangulation of short phase-coded pulses was used to track up to nine cod simultaneously inside a submerged Atlantic cod pen. The repetition time was between $1.7 - 3.3$ s using a 307.2 kHz carrier. Although 84.9 ± 1.2 % of the transmissions were successful in this study, the actual data rate was not mentioned. An example of a system using sensor tags is [12]. Fish-tag ID and depth information were transferred from two pens with 12, and 15 tagged Atlantic salmon, respectively. The transmission was repeated once every 90 s, and about 50 % of the transmissions were lost due to collisions, whereas 5–10 % was lost due to channel conditions. These tags took 4 s per transmission at a rate of a few bits per second, using a 69-kHz carrier and pulse-position modulation. A similar system from the same manufacturer was used in [14] to transfer depth and acceleration sensor data in separate messages from 21 tagged Atlantic salmon. In order to reduce collisions between tags, two separate frequency bands were used in the 69–71 kHz range. The repetition time was 220-380 s.

Monitoring fish effectively in pens requires a new system design to increase communication performance. Coherent acoustic communication has a rich history for other subsea applications [19] and allows for higher spectral efficiency, but requires compensation for intersymbol interference (ISI). A commonly used method to combat ISI in underwater communication is decision-feedback equalization with explicit phase tracking [20]. A single-channel equalizer is a powerful tool for mitigating channel distortions but has problems in rich scattering environments due to the rapid fading of channel taps. A hydrophone array can mitigate this problem. Multichannel equalizers can exploit the spatial diversity of the signal and thereby reduce ISI and fading of channel taps. Multichannel equalizers have been used with good results in a variety of underwater acoustic communication channels and frequency bands [e.g. 20].

The present paper demonstrates that is possible to meet the call for higher

bit rates, and thereby support a large number of tagged fish, by using coherent very high frequency[1] (VHF) communication in combination with array processing. Although multichannel equalizers improve communication performance by exploiting the spatial diversity, in addition to equalizing the channel, this is not enough. A fish telemetry system intended for aquaculture must be able to handle a large number of users.

The objectives of this paper are i) to characterize signal dispersion in time, frequency, and angle for a wideband VHF communication system with a center frequency of 250 kHz; ii) to determine the communication range and performance of a coherent high-speed scheme; iii) discuss the prospect of equipping a large number of fish with telemetry tags. The data in this paper come from measurements over a vertical link inside an Atlantic salmon net pen in August 2018.

The remainder of this paper is organized as follows. Section 2 describes the experiment. Channel properties for the Atlantic salmon pen acoustic channel are examined in section 3. The communication results are presented in section 4. The possibility to retrieve telemetry from a large number of tags and power constraints are discussed in section 4.4. Section 5 discusses the communication under other environmental conditions, conclusions are finally drawn in section 6.

2. Experimental setup

The experimental pen was one of four cylindrical net pens with a circumference of 157 m and a maximum depth of 40 m at the site (Fig. 1a). Each pen hosted 180 000 salmon with an average mass of 1.6 kg at the time of the experiment. If the fish were to be evenly distributed through the pen, this would correspond to approximately two individuals per cubic meter. However, the salmon tend to group together at higher densities depending on the current

[1] In this paper: low frequency $<$ 1 kHz, midfrequency 1–10 kHz, high frequency 10–100 kHz, and very high frequency $>$ 100 kHz.

external and internal environmental conditions [21]. Two factors that tend to concentrate fish in the upper layers of the pen are ongoing feeding [22, 23], notably early in the feeding period, and light conditions (summer months) [24]. Horizontally, the salmon tend to swim in a doughnut-shaped school during daytime [23, 24], avoiding the center of the pen.

In our case, the fish were being fed throughout the whole experiment and showed a high surface activity. Direct quantitative measurements of the fish density were not made, but visual inspection indicated that fish density was higher near the pen edge. The swimming speed of visible fish was estimated from video recordings at approximately one body length per second, with a preferred counter-clockwise swimming direction. The weather was calm with 0.2–0.3 m waves outside the pen and somewhat less inside. Fig. 1b shows a photo from the measurement site, where the receiver and transmitter were suspended from the red buoy. The buoy was moving back and forth with the surface waves at a frequency of about 0.5 hertz.

Details of the set-up can be seen in Fig. 2. It consisted of a single transmitter with a 30° opening angle, which was suspended in an adjustable rope under the receiver array. The receiver, 64 hydrophones arranged in a line array at a uniform spacing $< \lambda/2$ ($\lambda = 0.006$ m at 1500 m/s), was hanging 1 m under the buoy. The rear side of the receiver hydrophones was attached to a baffle structure, shielding the hydrophones from direct surface reflections. The measurement was conducted 5 m from the edge of the pen with Tx-Rx distances of 3, 8, 13 and 18 m.

The transmitted waveforms were binary phase-shift keying (BPSK) modulated, shaped with a root-raised-cosine filter with a 100 % roll-off, using a bit rate of 78.125 kbps and a carrier frequency of 250 kHz. A sequence of 4 waveforms was transmitted, consisting of 3 probe signals for channel sounding, and one pseudonoise communication sequence. The probe signals were cyclic maximal length (m-)sequences of length 255, 511 and 1023 bits. All waveforms had a duration of 4 s. They were transmitted with 1-s guard interval, making the whole sequence repetitive with a 20-s period. This transmit sequence was

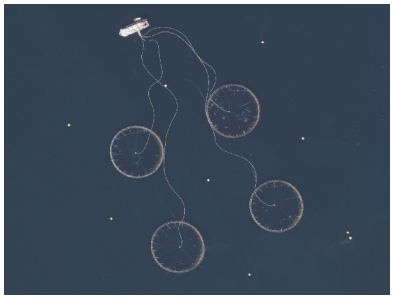

(a)

(b)

Figure 1: a) Aerial photo of the location, the pen in the upper right was used for the measurement. The pipes visible in and around the pens was used for pellet transportation. (Photo courtesy of Norge i bilder, Kartverket, Geovekst og kommunene.) b) Photo of the measurement site, the transmitter-receiver pair was suspended from the red buoy. A jumping salmon is noticed in the upper left of the photo.

repeated for at least 15 minutes at every Tx depth. The source level of the transmitter was approximately 178 dB re 1 μPa^{2}m^2.

3. The Atlantic Salmon pen acoustic channel

This section highlights characteristics of the VHF Atlantic salmon pen acoustic channel. The basis for the discussion is the time varying impulse response, $h(t,\tau)$, estimated through correlative channel sounding.

The acoustic channel is often modeled as a time-variant linear filter. Let $z(t)$ represent the transmitted complex baseband signal sampled at instants t. The received signal $y(t)$ is a distorted version of $z(t)$

$$y(t) = h(t,\tau) \circledast z(\tau) + e(t) \,, \tag{1}$$

where the acoustic channel effects are captured by $h(t,\tau)$, and where $e(t)$ represents noise.

Transmission of dedicated probe signals allows to estimate the impulse response. If the channel is linear and slowly time variant with respect to the m-sequence repetition period, the estimate of the channel impulse response $\hat{h}$

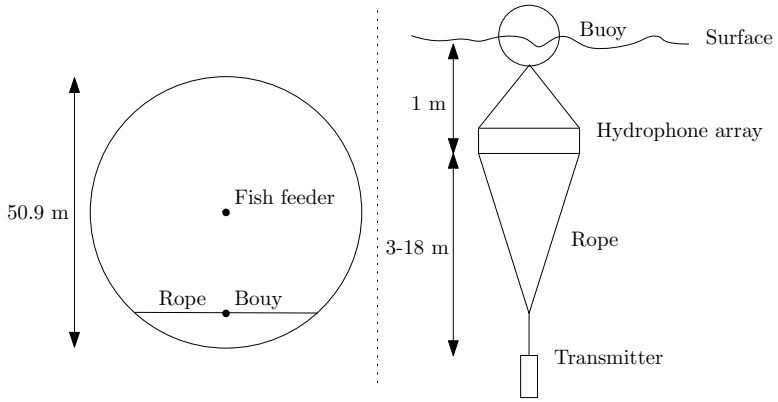

Figure 2: Set-up used for the measurements. The left sketch depicts the fish cage from above, and the right sketch illustrates the rope arrangement in which the transmitter and hydrophone array were suspended.

is the true channel, $h(t,\tau)$ convolved with the autocorrelation function of the channel probe $z(\tau)$

$$\hat{h}(t,\tau) = y(t) \circledast z^*(-\tau) = [h(t,\tau) \circledast z(\tau)] \circledast z^*(-\tau) \; . \tag{2}$$

The closer the autocorrelation $z(\tau) \circledast z^*(-\tau)$ of the transmitted signal is to a true impulse, the better the estimate of the channel will be. Using repetitive channel probes, an estimate of the channel impulse $\hat{h}(t,\tau)$, will be available for $t_n = nT$, where T is the probe repetition period and $n \in [0,1,2,\ldots N-1]$. The repetition rate T^{-1} has to be selected with care to minimize measurement errors. Temporal aliasing occurs when T is shorter than the delay spread, and frequency aliasing occurs when T^{-1} is smaller than the Doppler spread. m-sequence lengths of 255, 511 and 1023 bits were used, allowing measurements of Doppler spread up to 153, 76 and 38 Hz, and delay spreads up to 3, 6 and 13 ms, respectively.

An angularly resolved version of the impulse response is obtained by beamforming the responses obtained for the individual array elements. For a line array, using a standard delay-and-sum beamformer, the angularly resolved im-

pulse response estimate is

$$\hat{h}(t,\tau,\theta) = \sum_{m=1}^{M} \hat{h}_m(t,\tau - \Delta_m) \exp(\mathrm{i}2\pi\Delta_m f_c) \ , \tag{3}$$

where M is the number of hydrophones in the array, $\Delta_m = x_m \cdot \sin(\theta)/c$ with x_m denoting the hydrophone position in the array, and θ is the angle of arrival. For short ranges the element delay Δ_m has to be compensated for spherical spreading of the wavefront.

We will first provide the channel characteristics for a single element before proceeding to the angular characteristics. In the following single-element analysis element analysis, the center hydrophone ($m = 32$) of the array was used.

3.1. 1-D density functions

The power delay profile is $\mathbb{E}\left[|\hat{h}_{32}(t,\tau)|^2\right]$, and is estimated by averaging over the observation period NT

$$\hat{P}_{32}(\tau) = \frac{1}{NT} \int_0^{(N-1)T} \left|\hat{h}_{32}(t,\tau)\right|^2 \mathrm{d}t \ . \tag{4}$$

It is shown in Fig. 3a for the four vertical ranges. The curves are normalized by the value of the strongest arrival at the 3-m depth. The general structure of the delay profile is a direct arrival followed by a rich tail of scattered energy that lasts about 2 ms. As the depth increases, the direct arrival becomes weaker compared with the tail. Apart from the shortest range, most of the energy is received via scattered paths. At all depths, there is a bump in the delay profile between 4 and 8 ms. Delayed paths have traveled a longer distance. The delay between the direct path and the onset of the bump corresponds to an excess path length of 7.5 m at 3-m range, which decreases to 6 m at 18-m range. Geometric calculations show that this excess path length can be explained by reflection off the floating collar surrounding the pen. The excess path length is reduced as the angle from the transmitter towards the collar decreases, which occurs for a larger depth of the transmitter. This collar is a strong reflector that yields a measurable response even when the collar is outside the main lobe of the transmitter. The power carried by the bump is small compared to that of

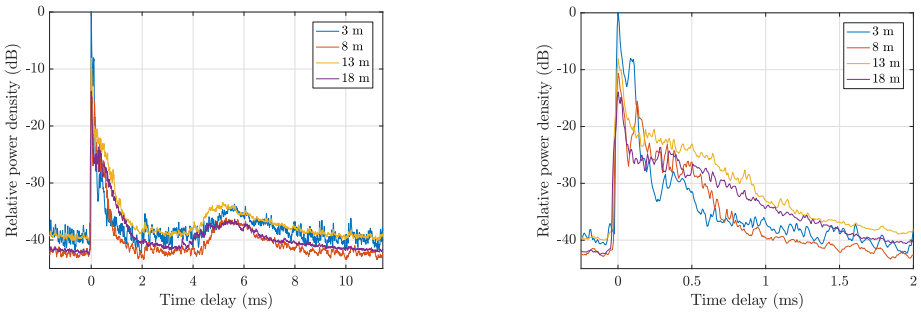

Figure 3: Power delay profile. (a) full range, (b) zoomed in on the first 2 ms.

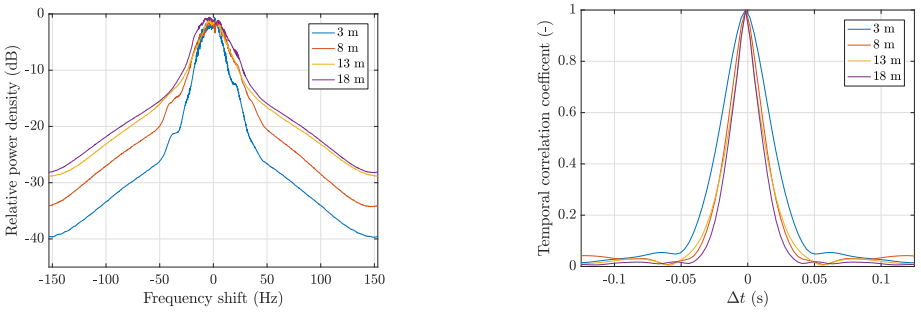

Figure 4: (a) Doppler power spectrum and (b) corresponding autocorrelation function.

the first 2 ms and is of little significance for communication performance. Fig. 3b zooms in on the start of the impulse response, highlighting the tail whose length increases with the depth up to 13 m depth.

The Doppler power spectrum is estimated as

$$\hat{P}_{32}(v) = \int_0^T \left| \int_0^{(N-1)T} \hat{h}_{32}(t,\tau) \exp(-2\pi \mathrm{i} v t) \mathrm{d}t \right|^2 \mathrm{d}\tau \tag{5}$$

and shown in Fig. 4a. The width of the spectrum increases with depth, as the fraction of energy received from moving scatterers in the water column increases. The main scatterers in this environment are most likely fish and food particles.

An important design parameter for coherent communication systems is the coherence time, which indicates at what rate the channel estimates have to be

refreshed in order to track fluctuations. The temporal correlation, here computed as the inverse Fourier transform of the Doppler power spectrum, is plotted in Fig. 4b. Defining the coherence time as the time it takes for the normalized correlation function to drop from 1 to 0.5, a value of ≈ 14 ms is found for depths beyond 3 m. In this fluctuating channel, communication has to occur in very short bursts, or the channel has to be continuously tracked.

3.2. 2-D density functions

The Doppler spectrum and the delay profile are informative quantities, but being 1-D density functions they do not reveal all channel characteristics contained in the time-varying impulse response. This section takes a closer look, using the transmission range of 18 m as an example.

The time-varying impulse response in Fig. 5a reveals an undulating first arrival that moves back and forth in delay with varying amplitude. This is more clearly shown in Fig. 6a, which zooms in on the first arrival. It is followed by a diffuse tail of weaker arrivals. The cycle period is 0.5 hertz and the peak-to-peak excursion in the delay is about 0.8 ms, corresponding to a path length variation of 0.12 m. There are periods of shadowing, in which the direct arrival can fade by as much as 20 dB, whereas the tail is much less affected. The periodic fading is present at all depths, occurs simultaneously on all hydrophones, and matches the period of the buoy movement.

The suspected cause of this behavior is a misalignment of the receiver caused by entangled ropes. The situation is depicted in Fig. 6b, where the receiver is mounted in a frame with the hydrophone array seen from the endfire direction. Owing to a mounting offset of the transmitter, the frame does not hang horizontally under the buoy, and as a result the frame will pivot around its left corner as the buoy moves up and down with the waves. The movement will be perpendicular to the hydrophone array. The pivoting will change the path length to the transmitter, as observed in Fig. 6a, and the angle of arrival. The change in angle is up to 40 degrees, which is enough to move the transmitter out of the main beam of the hydrophones. The fading will be strongest at the largest

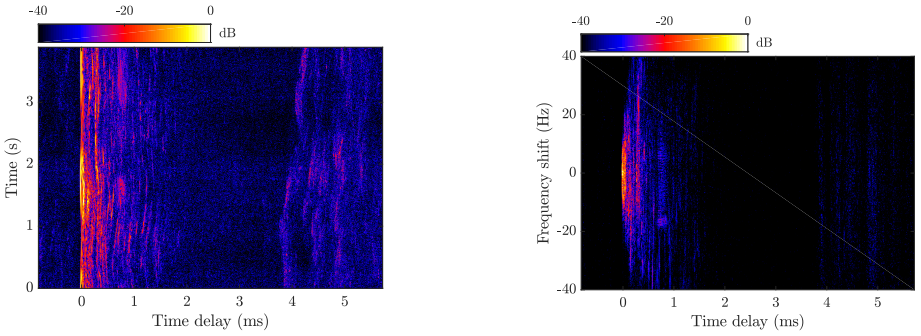

(a) (b)

Figure 5: (a) Impulse response and (b) delay-Doppler spread function measured at vertical distance of 18 m.

angular offset, corresponding to the longest excess path length, which matches well with what is seen in Fig. 6a. This also explains why all the hydrophones fade simultaneously, with a periodicity independent of transmitter depth. The fading is, therefore not a property of the acoustic channel, but rather an artifact of an improvised set-up.

The corresponding delay-Doppler spread function is shown in Fig. 5b. The Doppler spread is larger on delayed arrivals and is fairly evenly distributed around zero hertz. With ongoing feeding, the fish where highly mobile and could be a source of excess widening of the spectrum. There are distinct points in the scattering function, which could be reflections off fish moving at different velocities at different locations.

Figure 7 shows six snapshots of the angularly resolved impulse, evenly spaced throughout the 4-s probe signal. The magnitude is normalized on the strongest arrival across all snapshots and is clipped at -15 dB to highlight strong point scatterers. The $-10°$ offset of the direct arrival is caused by the misaligned set-up illustrated in Fig. 6b. The snapshots are characterized by a direct arrival and point scatterers which are sparsely distributed in the angle-delay domain. These scatterers are highly mobile and move around, appearing and disappearing between successive snapshots. The direct arrival is relatively stable by comparison.

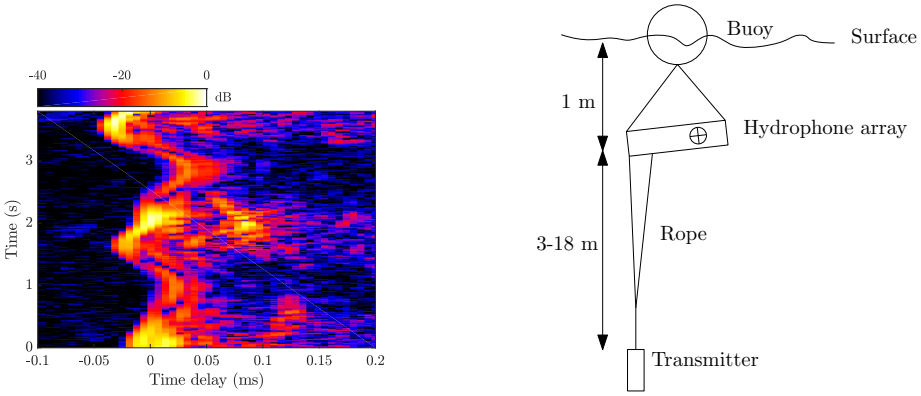

Figure 6: (a) Impulse response at 18 m depth, zoomed in on the first arrivals. Note that the fading only occurs during excess timedelays. (b) Maladjustment of the improvised set-up.

Although it wanders back and forth in delay, its angle varies only by a few degrees. The remainder of the energy arrives via a large number of weak point scatterers, which could be second-order reflections from fish or reflections off particles in the water column. The fish were being fed during the measurement; hence food particles might contribute. Angular dispersion and delay are not separable. Starting at 4 ms, the scatterers which cause the bump in Fig. 3a can be seen. These are also distinct point scatterers at various angles, presumably a reflection off the floating collar scattered back from the biomass.

3.3. Spatial correlation

The spatial correlation is important for a communication system with array processing. The receiver spatial correlation is defined as

$$Z_{m,m'} = \arg\max_{\Delta\tau} \frac{1}{T} \int_0^T \hat{h}_m^*(t,\tau)\hat{h}_{m'}(t,\tau+\Delta\tau)\mathrm{d}\tau \ , \tag{6}$$

and a normalized version

$$\hat{Z}_{m\hat{m}} = \frac{Z_{m\hat{m}}}{\sqrt{Z_{mm}Z_{\hat{m}\hat{m}}}} \ , \tag{7}$$

which is the maximum value of the cross correlation divided by the square root of the product of the peak autocorrelation values.

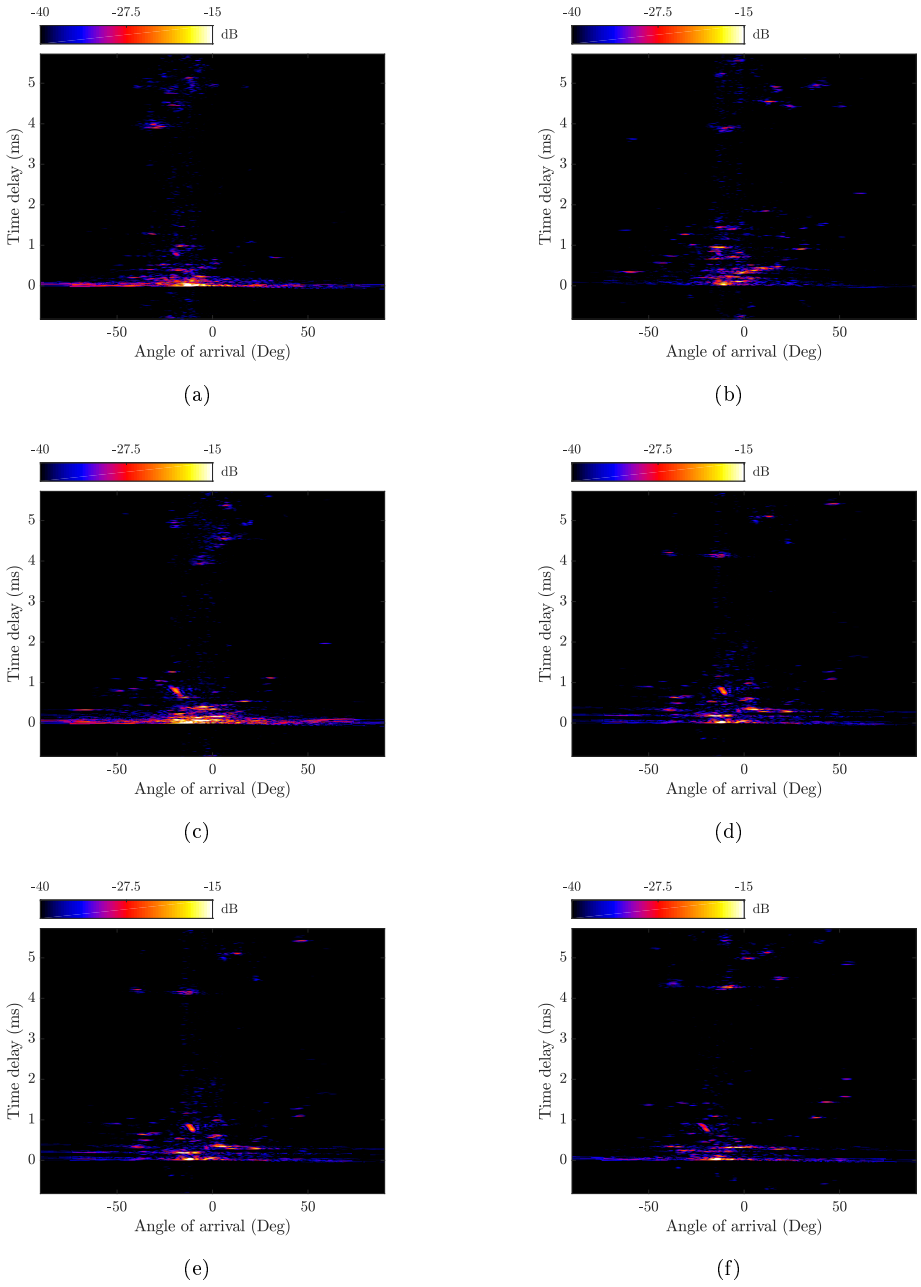

Figure 7: Snapshots of the angularly resolved impulse response at 18 meters depth, taken (a) 0 s, (b) 0.8, (c) 1.6, (d) 2.3, (e) 3.1 and (f) 3.8 s into the probe signal. The data are normalized on the strongest arrival across all snapshots and clipped at -15 dB.

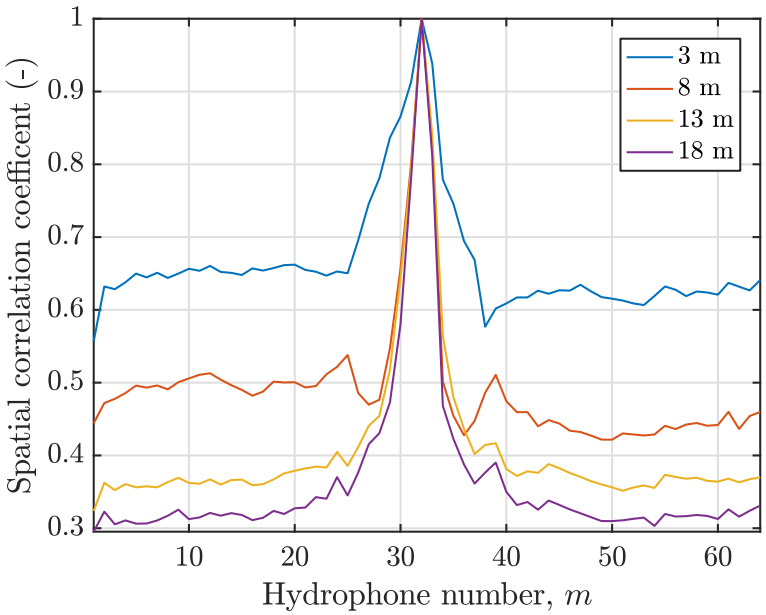

Figure 8: Average spatial correlation coefficient at four different depths .

The spatial correlation averaged over the whole measurement interval of the 64 hydrophones is plotted in Fig. 8, indicating that except for very short distances, the correlation is low. Using 0.5 as a criterion for uncorrelated signals, the signal spatial coherence length is about three hydrophone distances at 8, 13, and 18 m. At 3 m, the signal never decorrelates during the measurement interval. The reason for the low spatial coherence is that, except at 3 m, most of the energy is received via scattered paths. The contribution of noise to the measured decorrelation is negligible, as the SNR of the recorded signals exceeds 50 dB at all ranges.

The low spatial correlation indicates that diversity combining solutions may have an advantage over beamforming, yielding diversity gain with every third added hydrophone. On the other hand, the high SNR may permit harvesting sufficient energy from a single specular path with a beamformer, mitigating ISI by spatially filtering out diffuse scattered paths.

Table 1: Experiment conditions and parameters

Depth (m)	3	8	13	18
Input SNR per hydrophone (dB)	58	55	52	51
τ_{90} (ms)	0.14	0.69	2.18	3.2
τ_{50} (ms)	0.03	0.13	0.12	0.12
f_{90} (Hz)	37	42.1	58.6	70.7
f_{50} (Hz)	13.8	12.8	16.4	19.0
θ_{90} (degrees)	66.2	97.4	96.7	96.7
θ_{50} (degrees)	8.5	14.9	21.3	19.5
T_c (ms)	21	15	14	13
L_c (hydrophone spacing)	-	2.8	3	2.5

3.4. Summary of channel characteristics

The fish pen channel characteristics are summarized in Table 1. The depth is the vertical distance from the transmitter to the receiver. The delay (τ_{90} and τ_{50}), Doppler (f_{90} and f_{50}) and angular spread (θ_{90} and θ_{50}) are defined as the shortest intervals that contain 90 % respectively 50 % of the total received energy. The coherence time T_c and coherent length L_c is defined as the half peak width of the normalized correlation functions first 0.5 crossing points.

4. A receiver for short burst coherent communication

In previous sections, the VHF Atlantic salmon pen channel was presented. It is a highly fluctuating channel made up of direct arrival and strong point scatterers causing severe ISI, which renders coherent communication a challenging task. A well-established method to cope with ISI is multichannel equalization. Common approaches are either directly forwarding the hydrophone signals to a

multichannel equalizer, or by beamforming the hydrophone signals, forwarding one or several beams to the equalizer.

Multichannel equalizers can act as a beamformer and/or exploit spatial diversity, thereby reducing ISI and fading of channel taps, and have been used with good results in demanding underwater acoustic communication [e.g. 20].

A beamformer can steer beams towards distinct scatterers. This has been used with improved communication performance in the mid frequency band [25], here a reduced Doppler distortion and delay spread were reported, compared to the overall channel, when pointing narrow beams towards distinct angularly resolved arrivals. The drawback of beamforming is the requirement of high spatial coherence to obtain beamforming gain. When spatial coherence is low, the actual gain of beamforming will be limited. The spatial coherence for our channel was discussed in section 3.3 and showed a low spatial coherence for the three longest transmission ranges.

Two strategies are possible to deal with the short coherence time: i) communicate in short bursts, where the burst is shorter than the channel coherence time, or ii) use an adaptive receiver that tracks the channel. The first strategy is attractive for fish telemetry since the sensor data, for instance, swimming depth, heart rate, acceleration, and respiratory activity, require a packet size of a few bytes. The remaining section, therefore, focuses on a short-burst communication system that assumes a static channel during transmission.

4.1. Bit sequence

At a symbol rate of 78.125 kBd the channel will be decorrelated over ≈ 1100 symbols at a typical coherence time of 14 ms (Sec 3). The typical delay-spread which carries 50 % of the energy is <0.13 ms. Using these characteristics, a bit sequence consisting of 256 bits, whereof $L_t = 128$ bits are training and $L_p = 128$ are payload data, seems suitable and is well within the coherence time. This would give the pulse a 100 % overhead that negatively affects the effective bit rate and increases the collision probability, but it favors the channel estimate.

The communication performance is evaluated by processing the pseudorandom sequences as if it contained uncoded binary phase-shift keyed communication frames.

4.2. Receiver

The receiver in Fig. 9 uses an ordinary least-squares estimator to estimate the inverse channel that minimizes the error between the known transmitted training sequence and the received training sequence. The use of direct equalization combined with ordinary least-squares estimators is motivated by its robustness and simplicity, requiring no knowledge of the noise variance and statistical properties of the channel.

In the following discussion, it is assumed that the received signal has been brought to baseband and that the Doppler shift has been compensated for by adjusting the carrier, and if necessary using standard resampling prior to the receiver. Because the burst is very short, resampling will only be necessary in special cases. Frame synchronization is achieved by match-filtering for the pseudorandom training sequence at the start of the frame. The strongest peak in the filter output is taken as the start of the frame. The sampling rate into the receiver is $T_s = 2/T_b$ where T_b is the bit duration. The equivalent baseband signal is $y_m(t)$ and the kth discrete-time sample is $y_m(kT_s)$ (Fig. 9).

Let $\mathbf{Y}_{\hat{k},m}$ be the received signal synchronized on the start of training sequence, sample $\hat{k}$ at hydrophone m, arranged in matrix form

$$\mathbf{Y}_{\hat{k},m} = \begin{bmatrix} y_m([\hat{k} - L/2]T_s) & y_m([\hat{k} - L/2 + 1]T_s) & \dots & y_m([\hat{k} + L/2 - 1]T_s) \\ y_m([\hat{k} - L/2 + 2]T_s) & y_m([\hat{k} - L/2 + 3]T_s) & \dots & y_m([\hat{k} + L/2 + 1]T_s) \\ \vdots & \vdots & \vdots & \vdots \\ y_m([\hat{k} + L_t - L]T_s) & y_m([\hat{k} + L_t - L + 1]T_s) & \dots & y_m([\hat{k} + L_t - 1]T_s) \end{bmatrix}, \tag{8}$$

where $L = 39$ is the number of filter taps per hydrophone or beam and L_t is the length of the training sequence. The total number of taps is $64 \times 39 = 2496$ when all hydrophone channels are used. Stacking signal matrices from different

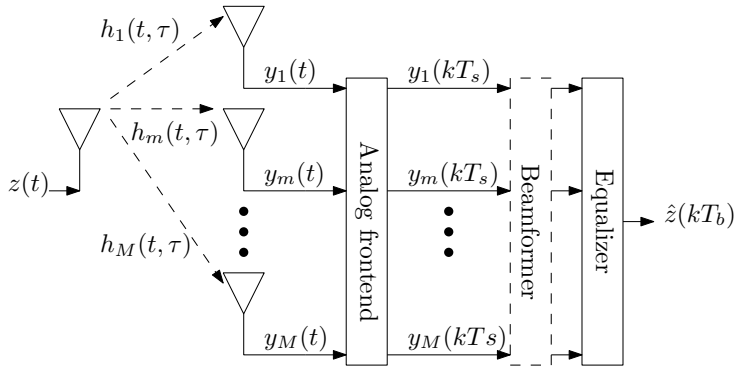

Figure 9: Equivalent baseband representation of receiver block diagram illustrating the three receiver strategies where the beamformer block can be activated, duplicated or completely bypassed.

hydrophones (or beams) gives the full received training signal matrix

$$\mathbb{Y}_{\hat{k}} = \left[\mathbf{Y}_{\hat{k},1}, \mathbf{Y}_{\hat{k},2}, \ldots \mathbf{Y}_{\hat{k},M} \right] . \tag{9}$$

The actual size of $\mathbb{Y}_{\hat{k}}$ depends on the number of used hydrophones or beams. In order to demodulate the payload, the set of filter coefficients which minimizes the error between known $\mathbf{z}_t$ and received training sequence $\mathbb{Y}_{\hat{k}}$ has to be found

$$\mathbf{g}_{\mathrm{LS}} = \arg \min_{\mathbf{g}} \| \mathbf{z}_t - \mathbb{Y}_{\hat{k}} \mathbf{g} \|^2 , \tag{10}$$

where $\mathbf{g}_{\mathrm{LS}}$ is a column vector with filter taps stacked for the different input channels, and $\mathbf{z}_t$ is the training bit sequence vector. The solution to (10) is

$$\mathbf{g}_{\mathrm{LS}} = \mathbb{Y}_{\hat{k}}^{+} \mathbf{z}_t , \tag{11}$$

where $^+$ denotes the pseudoinverse. A regularized inversion is used to increase the stability. An estimate of the transmitted payload bit vector is then

$$\hat{\mathbf{z}}_p = \mathbb{Y}_p \mathbf{g}_{\mathrm{LS}} \tag{12}$$

where $\mathbb{Y}_p$ has the same structure as $\mathbb{Y}_{\hat{k}}$ but contains the unknown payload part of the signal. Because of the short duration, neither adaptability nor a digital phase-locked loop showed any improvement, and were therefore omitted from the receiver.

4.3. Result and discussion

This section evaluates three different receiver designs, targeting fish telemetry in short bursts. All receivers use the equalizer described in the previous section, but they differ in the preprocessing stage. The first receiver uses a delay-and-sum beamformer to steer a narrow beam towards the strongest arrival. This receiver has the benefit of a small and deterministic beampattern, effectively suppressing out-of-beam interference. It has a low complexity as it feeds a single beam to the equalizer, it is hereafter denoted SBE (single beam equalizer). The second receiver has no preprocessing stage but instead directly feeds 64 hydrophones to a 64-channel equalizer, denoted MCE (multichannel equalizer). It has high complexity but enjoys the full flexibility of multichannel equalization. The third receiver is a hybrid combination, splitting the array into 16 subarrays, all steered in the direction of the strongest arrival. These beams serve as input to a 16-channel equalizer, denoted SAE (subarray equalizer). By splitting the array into 16 subarrays, each newly formed array contains four hydrophones, which is in agreement with the measured spatial coherence length. While being more complex than the SBE, it has lower complexity than the MCE.

4.3.1. Comparison of receiver strategies

Figure 10 shows the average output SNR for all equalizer strategies using a dataset of 800 frames for each depth. The MCE and SAE outperform the SBE for the same dataset and the same aperture. The SBE performs at best similar to the multichannel strategies, but never better in these channels. The difference between the SBE and multichannel strategies increases with the depth, in line with the reduction in spatial coherence seen in Fig. 8.

The MCE and SAE yield good results at all depths. As the depth increases, it may eventually be hard to maintain a useful output signal-to-noise ratio (SNR) ($\gtrapprox$ 6 dB) due to channel degradation, unless the array size increases. It is important to note that the degradation in output SNR solely comes from ISI, as the input SNR was $>$ 50 dB at all distances. The approach with the SAE

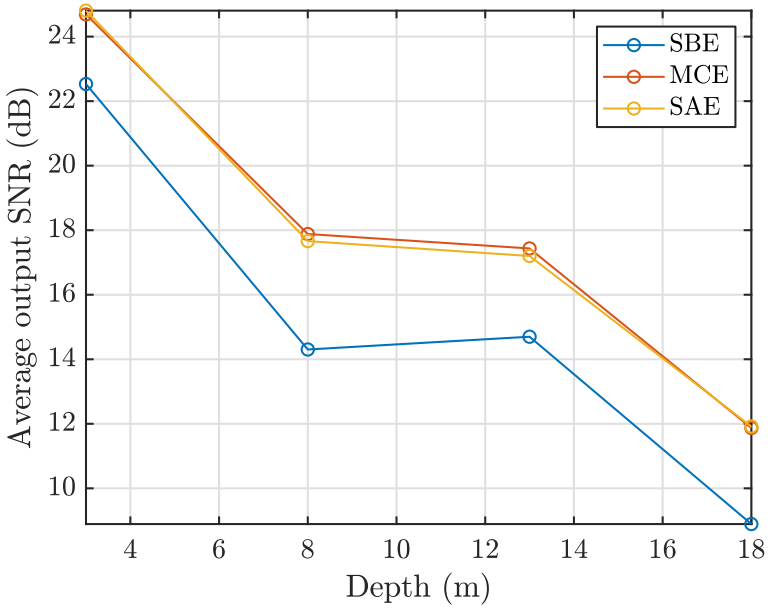

Figure 10: Comparison between the SBE (using the strongest beam), the MCE, and the SAE.

results in a marginal reduction in average output SNR compared to the MCE.

4.3.2. Angular response

In Fig. 10 the SBE output SNR came from the strongest beam, which is sub-optimal. Finding the beam with the highest output SNR is not always a trivial task, as it may differ from the strongest beam. This is exemplified in Fig. 11 which shows the unbiased receiver output SNR for the SBE and includes the beampattern for comparison. The direction of the highest output SNR coincides with either the highest or the second-highest peak in the beampattern. At short range, there is one dominant direction of arrival. As the depth increases, both the beampattern and output SNR obtain more structure, with several directions that could have been used for communication. However, the peaks are narrow, rendering the performance of a single-beam solution sensitive to pointing errors if the sequence gets longer, requiring the system to track the strongest beam adaptively.

To illustrate the difference between single and multichannel receiver strate-

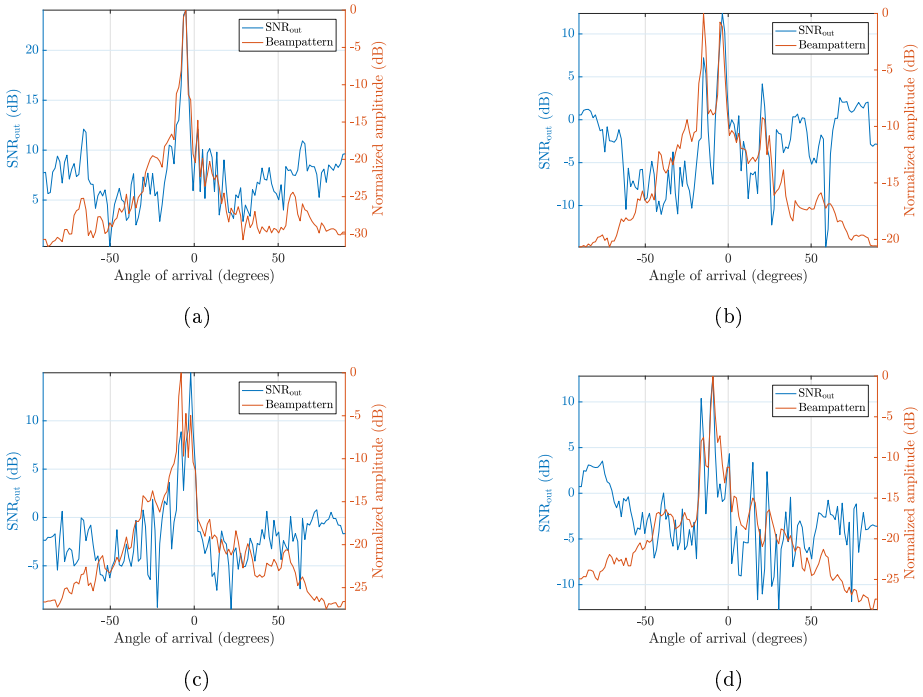

Figure 11: Beampattern obtained with a 64-element beamformer, and corresponding output SNR of the SBE. a) 3 m b) 8 m c) 13 m d) 18 m.

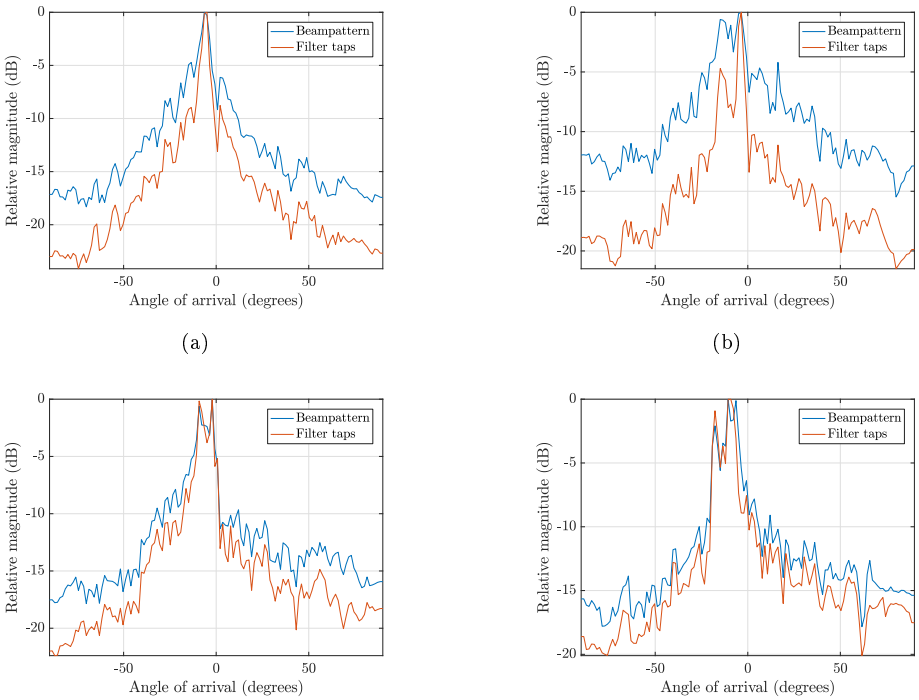

Figure 12: Beampattern and beamformed equalizer filter taps, a) 3 m b) 8 m c) 13 m d) 18 m. Note the match at increased depth.

gies, the MCE filter coefficients have been beamformed and are shown together with the beampattern in Fig. 12. At 3 m depth, there is a distinct main lobe in the same direction as the signal arrival, which indicates that the MCE coherently combines the channels, similar to the SBE. This explains why the average output SNRs at 3 m are close. As the depth increases and the spatial coherence reduces, the MCE beampattern widens and eventually matches the beamforming beampattern fairly well. This indicates that the MCE now works more like a diversity combiner where arrivals with different directions are coherently combined in the equalizer, unlike the SBE, which only uses one direction. This explains why the performance difference increases with depth.

The fact that the equalizer harvests most energy from a relatively narrow angular region suggests that it can be constrained, and does not require the full flexibility of 64 hydrophones with a relatively wide opening angle. Subarray beamforming, which is used in the SAE, results in beams with a smaller opening angle, with the benefit of i) a reduced receiver complexity ii) a higher input SNR into the equalizer, and perhaps most importantly, iii) reducing interference from out-of-beam arrivals. In order for subarray beamforming to be successful, the spatial coherence within the subarray has to be high. In this case, the subarray length slightly exceeds the spatial coherence length. The resulting loss was, however, negligible, as shown in Fig. 10.

4.3.3. Spatial response

As shown in Fig. 10, a MCE outperforms a SBE. The reason is its ability to exploit spatial diversity, as shown in section 3, giving it a significant advantage under difficult channel conditions. However, the performance of an MCE depends on the array configuration. Closely spaced hydrophones will be correlated, reducing the potential diversity gain. If the aperture is small, it will fail to pinpoint narrow arrivals, whereas a large spacing invokes grating lobes. The present section examines the array configuration. In doing so, we select M hydrophones from the set of 64 available hydrophones. The selection process considers either a fixed aperture or a fixed spacing; the latter results in an

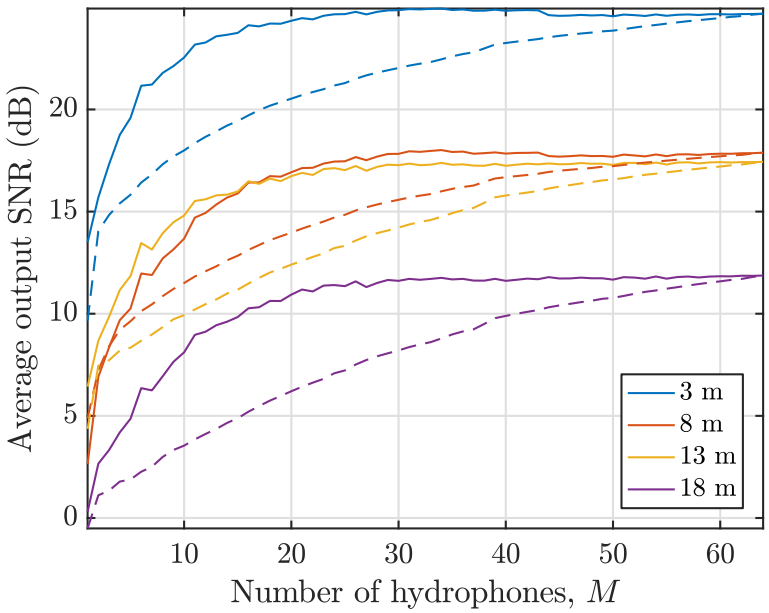

Figure 13: MCE receiver mean output SNR as function of number of active hydrophones, using two different methods to populate the array. 1) Solid line: fixed aperture, evenly filling the space between the end hydrophones ($m = 1$ and $m = 64$); 2) dashed line: fixed spacing.

aperture size that grows with M.

Figure 13 shows the communication performance in terms of output SNR improves with M, using the same 800 frames as in section 4.3.1. The fixed-aperture strategy increases rapidly with M and then flattens out. The gain is close to the full gain already at ≈ 20 hydrophones, which is in agreement with the measured spatial coherence length. The fixed-spacing strategy results in a steady increment of output SNR that matches the fixed-aperture method first when the array is fully populated. It appears that aperture is more important than the number of hydrophones. Indeed, closely spaced hydrophones provide essentially the same information to the receiver, and possibilities for spatial filtering are limited with wide beams.

Table 2: Received frames with one or more bit errors, for a SBE, SAE and MCE.

d, depth (m)	Frames received with bit errors (%)		
	SBE	SAE	MCE
3	0	0	0
8	8.6	0.75	0.12
13	26	12	12
18	43	26	27

4.3.4. Bit errors

The same 800 frames, as used in previous result, have been analysed for bit errors. The fraction of frames received with one or more bit errors are listed in Table 2. The first two ranges are basically error free for the SAE and MCE receiver. At 13 m frames with bit-error start to appear more frequency, and at 18 m the best result is 74 % error free frames. This was for the SAE, closely followed by the MCE with 73 % error free frames. The errors were most frequent in the periods of shadowing of the direct arrival. More than half of the erroneous frames had only one or two errors, which could be easily handled with a little source coding.

4.3.5. Communication during periods of shadowing

As shown in Fig. 5a the channels are characterized by periodic fading by as much as 20 dB. This shadowing predominantly affected the first arrival, increasing the relative strength of the reverberant tail. In Fig. 14 the output SNR has been calculated for short bursts (256 symbols whereof 128 symbols for training), repeated every 12 ms over the 4-s duration of the pseudorandom signal. It is clear that the output SNR is affected by the shadowing, and that the SBE is affected most, dropping by 20 dB. This indicates that the results presented in this paper might be overly pessimistic regarding the communication performance within a fish pen because the fading is a consequence of an improvised

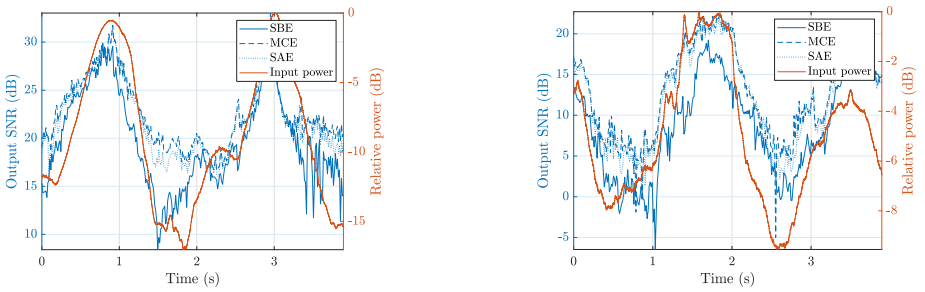

Figure 14: Instantaneous output SNR measured over 5 s shown together with hydrophone average input power at a) 3 m b) 18 m.

set-up.

4.4. Hypothetical fish telemetry system

It has been demonstrated that, with the help of a large hydrophone array, high-speed coherent burst communication is a viable approach for fish telemetry inside an Atlantic salmon pen. This section discusses the prospects of achieving real communication with a large number of tags, as called for in [4], and the tag power requirements.

4.4.1. Number of tags

Fish tags ought to be simple and lack any form of synchronization or channel sensing, simply transmitting at a fixed repetition rate. This will result in collisions when transmissions of multiple tags are received simultaneously. While some colliding tags can be resolved this will eventually limit the performance.

To give a lower bound, this section estimates the number of collision free fish tags per pen assuming a omnidirectional receiver. The burst length is 3.2 ms (256 symbols at 78.125 kBd), and each tag transmits at a repetition rate of 0.1 Hz, this gives 3052 available time slots. Here no distinction is made between fully or partially overlapping messages, this reduces the number of time slots to 1526. The probability of multiple transmissions in the same slot can be formulated as a ball and urn problem. The probability of getting exactly k

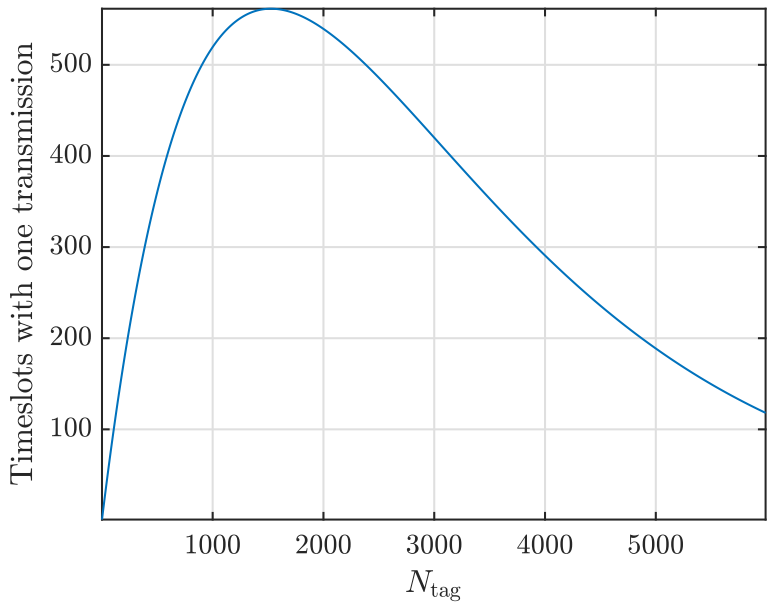

Figure 15: Number of collision-free slots for a varying number of tags.

transmissions in a specific time slot is given by the probability mass function of the binomial distribution

$$\Pr(X = k) = \binom{N_{\text{tag}}}{k} \left(\frac{1}{N_{\text{slot}}}\right)^k \left(1 - \frac{1}{N_{\text{slot}}}\right)^{N_{\text{tag}}-k} . \tag{13}$$

The expected number of time slots with one transmission is $\Pr(X = 1) \cdot N_{\text{slot}}$ and is shown in Fig. 15 as a function of the number of tags and available time slots. A few hundred tags can be handled before collisions are noticed. The number of read tags will continue to grow until $N_{\text{tag}} \approx 1500$, but at this point, more than half of the tags will experience collisions. Beyond 1500 tags the throughput starts to decline. By reducing the tag transmission repetition rate, or by introducing angular sectors, the effective number of time slots increases.

4.4.2. Power requirement

There will be a strict power requirement on the fish telemetry tags. For practical reasons, the battery cannot be replaced and has to last for the whole deployment, which is up to two years. The input SNR was very high at all ranges

in our experiment (Table 1), and the performance was not limited by noise but by ISI. The source level of the transmitter was 178 dB re 1 μPa^2m^2. The question arises how much the transmit power can be reduced without affecting the performance. The VHF regime is characterized by thermal noise, which is white. Hence, in order to test noise resilience, white Gaussian noise was added to the recordings. The result is plotted in Fig. 16. The reference curve is the 64-hydrophone equalizer curve from Fig. 10, for which the input SNR exceeded 50 dB at all ranges. The other curves demonstrate that the input SNR can be reduced by at least 40 dB before the performance is affected (an output SNR of $\approx$10 dB is sufficient for BPSK, or $\approx$ 6 dB with some coding). This is equivalent to a transmitter source level of 138 dB re 1 μPa^2m^2. For an omnidirectional lossless transducer, this corresponds to 0.3 mW of electrical power.

At a symbol rate of 78.125 kBd, and a frame length of 256 bits, the energy per transmission is 1 µJ for an omnidirectional lossless 0.3 mW transducer, and at a repetition rate of 0.1 hertz, the total energy required for a two-year deployment is 6 J which is well within reach of existing battery technology. If we, for example, extend the range from 18 m to 100 m, the extra propagation loss is about 20 dB, assuming spherical spreading and an absorption of about 6 dB per 100 m at 250 kHz in seawater. The increment of 20 dB in source level corresponds, in our example tag, to 30 mW of electrical power, and energy consumption of 600 J for a two year deployment. The energy requirement for acoustical fish tag telemetry is not a limiting factor.

5. Discussion

During the field test, the weather conditions were relatively benign. The experiments were performed over a vertical channel, using a receiver shielded for surface reflections. Following a strong direct path, there was a diffuse tail of weaker arrivals ascribed to scattering by fish and the pen construction. The main cause of bit errors was shadowing of the direct path due to receiver misalignment and motion by surface waves.

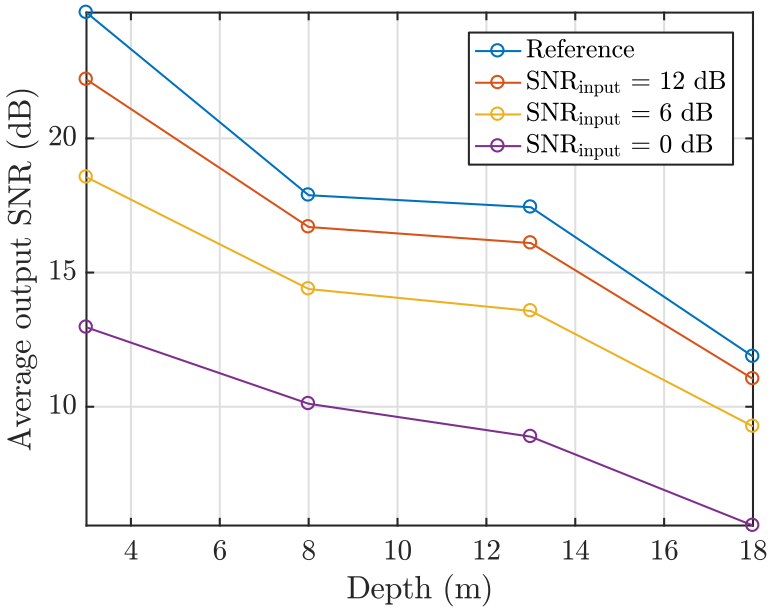

Figure 16: Output SNR as function of depth for four different input SNR noise levels. The reference curve is the actual measured output SNR.

An operational system will be working under different conditions. A big difference is that the majority of links will be slant channels, which may invoke more multipath propagation than vertical channels in a shallow-water environment. However, multipath due to surface and bottom reflections is not expected in our scenario. The employed baffle attenuates all sound from angles exceeding 90° (measured from the direction pointing down from the receiver), and thus blocks surface directions also in slant channels. The receiver array is usable to about 80°, and can serve most of the salmon, except those very close to the surface. Bottom reflections will be unimportant, because of the large excess path length and the strong absorption at these high frequencies.

An environmental condition that can challenge the proposed communication system is wind-induced surface gravity waves. Although the floating collar attenuates waves to some extent, significant waves can exist inside a pen. Shadowing of the direct path can be avoided with a proper deployment, but

wave-induced instrument motion can lead to large Doppler effects. As the wind speed increases, breaking waves may infer clouds of air bubbles in the surface layer [e.g. 26]. While being most prominent in the first few meters, there is evidence that bubbles can be drawn down to depths of 10–20 m [26, 27] through Langmuir circulation. Air bubbles have a screening effect through scattering and absorption of sound. The strength of the screening depends on the bubble concentration, the bubble size distribution, and the acoustic frequency. The effect of wave motion and bubbles on the link quality is hard to predict, but could be mitigated by fixing the receiver to the pen construction, at some depth. On the other hand, this may require removal of the baffle in order to receive tags from above the receiver, simultaneously inviting surface reflections. Results cited by [21] suggest that fish swim deep during storms, which is an argument for a deep receiver.

Crowding is another factor that will affect the acoustic channel. Crowding is a process in the production cycle where the available size of the pen is reduced, and fish are constrained to a smaller volume. Crowding occurs in connection with loading to well boat and medical treatment. From an acoustic point of view, the higher fish density during crowding increases the density of scatterers. Low-rate incoherent communication was demonstrated during crowding in [14], using eight unsynchronized receivers around the pen.

How high-speed coherent communication is affected by different operational scenarios and environmental conditions has to be further examined. The results from our initial experiment are promising, and measures can be taken to ensure throughput also during more challenging conditions. For instance, multiple receivers could be deployed to serve different sectors of the pen, either horizontally and/or vertically separated. Although technically feasible, the practical and economical feasibility of more complex systems also has to be evaluated.

6. Conclusion

Utilizing data from a field test in Bergen, Norway, August 2018, a VHF acoustic channel inside an Atlantic salmon pen has been characterized at different ranges. The time-varying impulse response was estimated with a correlative channel sounder and characterized in terms of Doppler spread, delay spread, angular spread, and spatial and temporal coherence. The pen channel is highly dynamic with a delay spread of several ms and a coherence time as short as 13 ms.

A high-speed coherent burst communication system for fish telemetry has been evaluated, where a 64-channel non-adaptive channel equalizer reveals a satisfactory performance for transmission ranges up to 18 m (the longest tested range). Calculations illustrate the prospect of retrieving data in real time from a large number of tagged fish. It appears technically possible and feasible to use high-speed coherent communication in the VHF band for fish telemetry inside Atlantic salmon pens.

Further research topics are the communication performance under different processes in the production cycle, under harsh weather conditions, different receiver configurations, and finally the required coverage and number of tagged fish.

Acknowledgment

We thank the staff at Lerøy Seafood and NCE Seafood Innovation for being central in acquiring the field data for this paper. Special thanks to Harald Sveier for making the fish farm available and to Björgólfur Hávarðsson for help with ropes.

Comments by three anonymous reviewers helped to improve the manuscript on several counts.

Founding

This work was supported by the Norwegian Research Council under Project 251828.

References

[1] FOA, The State of World Fisheries and Aquaculture 2018 – Meeting the sustainable development goals (2018).
URL http://www.fao.org/3/i9540en/I9540EN.pdf

[2] H. V. Bjelland, M. Føre, P. Lader, D. Kristiansen, I. M. Holmen, A. Fredheim, E. I. Grøtli, D. E. Fathi, F. Oppedal, I. B. Utne, I. Schjølberg, Exposed aquaculture in norway, in: OCEANS 2015 - MTS/IEEE Washington, 2015, pp. 1–10.

[3] P. J. Ashley, Fish welfare: Current issues in aquaculture, Applied Animal Behaviour Science 104 (3) (2007) 199 – 235, fish Behaviour and Welfare. doi:https://doi.org/10.1016/j.applanim.2006.09.001.
URL http://www.sciencedirect.com/science/article/pii/S0168159106002954

[4] M. Føre, K. Frank, T. Norton, E. Svendsen, J. A. Alfredsen, T. Dempster, H. Eguiraun, W. Watson, A. Stahl, L. M. Sunde, C. Schellewald, K. R. Skøien, M. O. Alver, D. Berckmans, Precision fish farming: A new framework to improve production in aquaculture, Biosystems Engineering 173 (2018) 176 – 193, advances in the Engineering of Sensor-based Monitoring and Management Systems for Precision Livestock Farming. doi:https://doi.org/10.1016/j.biosystemseng.2017.10.014.
URL http://www.sciencedirect.com/science/article/pii/S1537511017304488

[5] E. Thorstad, A. Rikardsen, A. Alp, F. Økland, The use of electronic tags in fish research–an overview of fish telemetry methods, Turkish Journal of Fisheries and Aquatic Sciences 13 (5) (2013) 881 – 896.

[6] S. J. Cooke, S. G. Hinch, M. Wikelski, R. D. Andrews, L. J. Kuchel, T. G. Wolcott, P. J. Butler, Biotelemetry: a mechanistic approach to ecology, Trends in Ecology & Evolution 19 (6) (2004) 334 – 343. doi:https://doi.org/10.1016/j.tree.2004.04.003.
URL http://www.sciencedirect.com/science/article/pii/S0169534704001120

[7] C. Rillahan, M. Chambers, W. H. Howell, W. H. Watson, A self-contained system for observing and quantifying the behavior of Atlantic cod, Gadus morhua, in an offshore aquaculture cage, Aquaculture 293 (1) (2009) 49 – 56. doi:https://doi.org/10.1016/j.aquaculture.2009.04.003.
URL http://www.sciencedirect.com/science/article/pii/S0044848609003330

[8] J.-E. Juell, H. Westerberg, An ultrasonic telemetric system for automatic positioning of individual fish used to track atlantic salmon (salmo salar l.) in a sea cage, Aquacultural Engineering 12 (1) (1993) 1 – 18. doi:https://doi.org/10.1016/0144-8609(93)90023-5.
URL http://www.sciencedirect.com/science/article/pii/0144860993900235

[9] M. Føre, J. A. Alfredsen, A. Gronningsater, Development of two telemetry-based systems for monitoring the feeding behaviour of Atlantic salmon (Salmo salar L.) in aquaculture sea-cages, Computers and Electronics in Agriculture 76 (2) (2011) 240 – 251. doi:https://doi.org/10.1016/j.compag.2011.02.003.
URL http://www.sciencedirect.com/science/article/pii/S0168169911000536

[10] J. Kolarevic, . Aas-Hansen, . Espmark, G. Baeverfjord, B. F. Terjesen, B. Damsgård, The use of acoustic acceleration transmitter tags for monitoring of atlantic salmon swimming activity in recirculating aquaculture systems (ras), Aquacultural Engineering 72-73 (2016) 30 – 39.

doi:https://doi.org/10.1016/j.aquaeng.2016.03.002.
URL http://www.sciencedirect.com/science/article/pii/S0144860916300450

[11] I. G. Priede, A. H. Young, The ultrasonic telemetry of cardiac rhythms of wild brown trout (Salmo trutta L.) as an indicator of bio-energetics and behaviour, Journal of Fish Biology 10 (4) (1977) 299–318. arXiv:https://onlinelibrary.wiley.com/doi/pdf/10.1111/j.1095-8649.1977.tb04064.x, doi:10.1111/j.1095-8649.1977.tb04064.x.
URL https://onlinelibrary.wiley.com/doi/abs/10.1111/j.1095-8649.1977.tb04064.x

[12] M. Føre, K. Frank, T. Dempster, J. Alfredsen, E. Høy, Biomonitoring using tagged sentinel fish and acoustic telemetry in commercial salmon aquaculture: A feasibility study, Aquacultural Engineering 78 (2017) 163 – 172. doi:https://doi.org/10.1016/j.aquaeng.2017.07.004.
URL http://www.sciencedirect.com/science/article/pii/S0144860917300432

[13] E. Baras, J.-P. Lagardère, Fish telemetry in aquaculture: review and perspectives, Aquaculture International 3 (2) (1995) 77–102. doi:10.1007/BF00117876.
URL https://doi.org/10.1007/BF00117876

[14] M. Føre, E. Svendsen, J. Alfredsen, I. Uglem, N. Bloecher, H. Sveier, L. Sunde, K. Frank, Using acoustic telemetry to monitor the effects of crowding and delousing procedures on farmed atlantic salmon (salmo salar), Aquaculture 495 (2018) 757 – 765. doi:https://doi.org/10.1016/j.aquaculture.2018.06.060.
URL http://www.sciencedirect.com/science/article/pii/S0044848617324407

[15] P. A. van Walree, Propagation and Scattering Effects in Underwater Acous-

tic Communication Channels, IEEE Journal of Oceanic Engineering 38 (4) (2013) 614–631. doi:10.1109/JOE.2013.2278913.

[16] R. E. Francois, G. R. Garrison, Sound absorption based on ocean measurements. Part II: Boric acid contribution and equation for total absorption, J. Acoust. Soc. Am. 72 (6) (1982) 1879–1890.

[17] J. A. Hildebrand, Anthropogenic and natural sources of ambient noise in the ocean, Marine Ecology Progress Series 34 (12) (2009) 1936–1956.

[18] C. Radford, M. Slater, Soundscapes in aquaculture systems, Aquaculture Environment Interactions 11 (2019) 53 – 62.

[19] D. B. Kilfoyle, A. B. Baggeroer, The state of the art in underwater acoustic telemetry, IEEE Journal of Oceanic Engineering 25 (1) (2000) 4–27. doi:10.1109/48.820733.

[20] M. Stojanovic, J. A. Catipovic, J. G. Proakis, Phase-coherent digital communications for underwater acoustic channels, IEEE Journal of Oceanic Engineering 19 (1) (1994) 100–111. doi:10.1109/48.289455.

[21] F. Oppedal, T. Dempster, L. H. Stien, Environmental drivers of Atlantic salmon behaviour in sea-cages: A review, Aquaculture 311 (1) (2011) 1 – 18. doi:https://doi.org/10.1016/j.aquaculture.2010.11.020.
URL http://www.sciencedirect.com/science/article/pii/S0044848610007933

[22] A. Fernö, I. Huse, J.-E. Juell, Åsmund Bjordal, Vertical distribution of Atlantic salmon (Salmo solar L.) in net pens: trade-off between surface light avoidance and food attraction, Aquaculture 132 (3) (1995) 285 – 296. doi:https://doi.org/10.1016/0044-8486(94)00384-Z.
URL http://www.sciencedirect.com/science/article/pii/004484869400384Z

[23] J.-E. Juell, A. Fernö, D. Furevik, I. Huse, Influence of hunger level and food availability on the spatial distribution of Atlantic salmon,

Salmo salar L., in sea cages, Aquaculture Research 25 (4) (1994) 439–451. arXiv:https://onlinelibrary.wiley.com/doi/pdf/10.1111/j.1365-2109.1994.tb00709.x, doi:10.1111/j.1365-2109.1994.tb00709.x.
URL https://onlinelibrary.wiley.com/doi/abs/10.1111/j.1365-2109.1994.tb00709.x

[24] F. Oppedal, J.-E. Juell, G. L. Tarranger, T. Hansen, Artificial light and season affects vertical distribution and swimming behaviour of post-smolt Atlantic salmon in sea cages, Journal of Fish Biology 58 (6) (2001) 1570–1584. arXiv:https://onlinelibrary.wiley.com/doi/pdf/10.1111/j.1095-8649.2001.tb02313.x, doi:10.1111/j.1095-8649.2001.tb02313.x.
URL https://onlinelibrary.wiley.com/doi/abs/10.1111/j.1095-8649.2001.tb02313.x

[25] J. Li, Y. V. Zakharov, Efficient Use of Space-Time Clustering for Underwater Acoustic Communications, IEEE Journal of Oceanic Engineering PP (99) (2017) 1–11. doi:10.1109/JOE.2017.2688558.

[26] S. A. Thorpe, G. E. R. Deacon, On the clouds of bubbles formed by breaking wind-waves in deep water, and their role in air-sea gas transfer, Philosophical Transactions of the Royal Society of London. Series A, Mathematical and Physical Sciences 304 (1483) (1982) 155–210. doi:10.1098/rsta.1982.0011.

[27] D. Farmer, M. Li, Patterns of bubble clouds organized by langmuir circulation, Journal of Physical Oceanography 25 (6) (1995) 1426–1440. doi:10.1175/1520-0485(1995)025<1426:POBCOB>2.0.CO;2.